Title
Estimating long-term multivariate progression from short-term data

Journal
Alzheimer's & Dementia, 10(5 Suppl)

ISSN
1552-5260

Authors
Donohue, Michael C
Jacqmin-Gadda, Hélène
Le Goff, Mélanie
et al.

Publication Date
2014-10-01

DOI
10.1016/j.jalz.2013.10.003

Peer reviewed

Published in final edited form as:
Alzheimers Dement. 2014 October ; 10(0): S400–S410. doi:10.1016/j.jalz.2013.10.003.

Estimating long-term multivariate progression from short-term data

Michael C. Donohue[a], **Helene Jacqmin-Gadda**[b], **Mélanie Le Goff**[b], **Ronald G. Thomas**[a,h], **Rema Raman**[a,h], **Anthony C. Gamst**[a,h], **Laurel A. Beckett**[c], **Clifford R. Jack Jr**[d], **Michael W. Weiner**[e], **Jean-Francois Dartigues**[c], and **Paul S. Aisen**[g] **for the Alzheimer's Disease Neuroimaging Initiative**[h]

[a]Department of Family and Preventive Medicine, Division of Biostatistics and Bioinformatics, University of California San Diego, La Jolla, CA 92093, USA

[b]INSERM, U897, Biostatistics Department, Bordeaux, F-33076, France

[c]Department of Public Health Sciences, Biostatistics Unit, University of California Davis, Davis, CA 95616, USA

[d]Department of Radiology, Mayo Clinic, Rochester, MN 55902, USA

[e]Center for Imaging of Neurodegenerative Diseases, University of California, San Francisco

[f]INSERM, U897, Aging Department, Bordeaux, F-33076, France

[g]Department of Neuroscience, University of California San Diego, La Jolla, CA 92093, USA

[h]Data used in preparation of this article were obtained from the Alzheimers Disease Neuroimaging Initiative (ADNI) database (http://adni.loni.usc.edu). As such, the investigators within the ADNI contributed to the design and implementation of ADNI and/or provided data but did not participate in analysis or writing of this report. A complete listing of ADNI investigators can be found at: http://adni.loni.usc.edu/wp-content/uploads/how_to_apply/ADNI_Acknowledgement_List.pdf

Abstract

Motivation—Diseases that progress slowly are often studied by observing cohorts at different stages of disease for short periods of time. The Alzheimer's Disease Neuroimaging Initiative (ADNI) follows elders with various degrees of cognitive impairment, from normal to impaired. The study includes a rich panel of novel cognitive tests, biomarkers, and brain images collected every six months for up to six years. The relative timing of the observations with respect to disease pathology is unknown. We propose a general semi-parametric model and iterative estimation procedure to simultaneously estimate pathologic timing and long-term growth curves.

Contact: mdonohue@ucsd.edu.

The resulting estimates of long-term progression are fine-tuned using cognitive trajectories derived from the long-term “Personnes Agées QUID” (PAQUID) study.

Results—We demonstrate with simulations that the method can recover long-term disease trends from short-term observations. The method also estimates temporal ordering of individuals with respect to disease pathology, providing subject-specific prognostic estimates of the time until onset of symptoms. When the method is applied to ADNI data, the estimated growth curves are in general agreement with prevailing theories of the Alzheimer’s disease cascade. Other datasets with common outcome measures can be combined using the proposed algorithm.

Availability—Software to fit the model and reproduce results with the statistical software R is available as the grace package (http://mdonohue.bitbucket.org/grace/). ADNI data can be downloaded from the Laboratory of NeuroImaging (http://loni.usc.edu).

Keywords

multiple outcomes; semiparametric regression; self modeling regression

1. Introduction

Several methods exist for estimating smooth progression or growth curves from serial observations of individuals over some biologically common time span. For example, generalized linear or nonlinear mixed effects models [1] can be used to model height, weight, or pharmacokinetics over time from some event of interest. The event might be birth or an intervention. However, we often study diseases that occur over long periods of time by sampling populations at different stages of disease and taking short-term longitudinal “snapshots”. Epidemiological studies with biologically heterogeneous subpopulations may not have an obvious biological event than can serve as a reference “time zero”. Such a “time zero” is required to fit the standard mixed-effects model. Also, the standard nonlinear mixed-effects models and software assume similar features on both the subject and population levels [1, 2, 3]. Short-term follow-up with relatively few observations may require much simpler subject-level features.

A motivating example is Alzheimers Disease (AD), which is believed to develop decades before the onset of symptoms. The Alzheimers Disease Neuroimaging Initiative (ADNI, adni-info.org) has followed volunteers diagnosed as Cognitively Normal (CN), Early and Late Mild Cognitive Impairment (EMCI and LMCI), and probable mild AD. Maximum follow-up is up to about 6 years at present and data collection is ongoing. The ADNI battery includes serial magnetic resonance imaging (MRI) measures of regional brain volumes, positron emission tomography (PET) measures of brain function and amyloid accumulation, other biological markers, and clinical and neuropsychological assessment. Time of onset of dementia, a potential “time zero”, is recorded for subjects with, or transitioning to, dementia, but these times can be unreliable and subjective. Furthermore, CN and MCI individuals may not be followed long enough to observe clinical transitions.

Jack et al. [4, 5] proposed a long-term model of the AD pathological cascade, and specifically hypothesized the trajectory of several key biomarkers over the decades

preceding the onset of dementia symptoms. The model (Figure 1) proposes that the AD cascade begins many years prior to the onset of symptoms with amyloid plaque deposition in the brain followed by neurofibrillary tau tangles; cognitive, clinical and functional decline are relatively late features of the disease. This hypothesized model is shaping the field of AD research. Drug development and observational studies have shifted focus to earlier stages of the disease, selecting subjects not on symptomatic impairment, but on biomarker signatures. Ideally we would test the hypothesized model by enrolling a large cohort of CN subjects and collecting biomarkers and cognitive and functional assessments over decades. The subset who progress to AD could be used to model the long-term biomarker progression of the disease. Until such a study is conducted, we are limited to analyzing shorter-term studies, such as ADNI.

Self modeling regression (SEMOR) is an approach for fitting sets of curves under the assumption of a common shape [6]. A subclass of SEMOR, shape invariant models [7, 8, 9, 10], accommodate unknown location and scale parameters for both the outcome and the time covariate and model the common shape with regression splines. Kneip and Gasser [6] relaxed some of the parametric assumptions by using kernel smoothers to estimate the common shape. Others have modeled the common shape with free-knot regression splines [11], smoothing splines [12], and penalized splines [13, 14, 15].

To our knowledge, SEMOR has only been applied to datasets in which each subject has similar follow-up. SEMOR approaches assume a common shape over the population, and estimate subject-level curves with similar features as the population curve. Our goal is to estimate population curves over decades of AD progression on an array of outcome measures; but subject-level data is comprised of at most 9 observations over 6 years. We propose a SEMOR model with simple linear subject-level effects, while modeling long-term features with non-parametric monotone smoothing. Subjects are shifted backward or forward in time according to performance across the panel of outcomes. Long-term progression curves for the multiple outcomes, and subject-specific random-effects and time shifts, are iteratively estimated until convergence of the residual sum of squares.

There have been studies of AD progression with long-term follow-up, but these tend to lack the novel biomarkers of prime interest in early stages of the disease. For instance, the “Personnes Agees QUID” (PAQUID) study has followed 3,777 French individuals aged 65 years or older studied from 1988 until present [16]. The PAQUID dataset lacks the imaging and cerebrospinal fluid biomarkers that ADNI collected, but provides invaluable long-term MMSE trajectories [17]. We can use these trajectories to fine-tune the results of the algorithm applied to ADNI data, and transform time to represent time-to-dementia-onset.

2. Model assumptions

We assume several outcomes Y_{ij} arise over time t, for individual $i = 1,\ldots, n$ and outcome $j = 1,\ldots, m$, according to:

(1)

Furthermore, we assume each g_j is a continuously differentiable monotone function, γ_i have mean 0 and variance  , $(\alpha_{0ij}; \alpha_{1ij})$ are bivariate Gaussian with mean 0 and covariance matrix Σ_j, and $\varepsilon_{ij}(t)$ are independent Gaussian residual errors with mean 0 and outcome-specific variance σ_j. To simplify notation, we think of t as both a covariate and a continuous valued index. "Short-term" observation time is represented by observed covariate t. In a panel study like ADNI, t would correspond to the study-time clock. "Long-term" progression time is represented by $t + \gamma_i$, where γ_i is the unknown subject-specific time shift. If subjects aged uniformly, with identical ages at different stages of progression of the underlying disease features, "long-term" progression time would be the subjects age; in fact, however, disease manifests at different ages, so this corresponds to an unknown "health-age", which may be shifted left or right relative to actual age.

Panel A of Figure 2 depicts simulated data generated according to (1). The logistic function $g_1(t) = 1/(1 + \exp(-t))$, the linear function $g_2(t) = t/12 + 0{:}5$ and the quadratic $g_3(t) = (t + 6)^2/72$ generated the three outcomes. For each of the 100 subjects, we sampled subject-specific time shifts, γ_0, uniformly from the interval −5 to 5. The unshifted observation times were $t = -1, -0.5, 0, 0.5, 1$. The random intercepts and slopes for each subject and outcome are distributed according to a bivariate Gaussian with mean 0, variance 0.01, and covariance 0.005. The residual variance is also Gaussian with variance 0.01. We chose the different long-term shapes to test whether our semi-parametric method could recover them without supervision. The observation times and long-term scatter were chosen to roughly mimic ADNI. The variance parameters were chosen so that the long-term trends were reasonably apparent by visual inspection of Panel A of Figure 2.

The long-term trends are obvious in Panel A of Figure 2 because the data are plotted with the simulated time shifts. However, the time shifts are not observed in data like ADNI. Rather, the data is observed as in Panel B of Figure 2. The goal of the algorithm proposed in the next section is to estimate both the time shift parameters and the long-term curves. The algorithm will leverage the assumption that the long-term trends are monotone and pool information across outcomes to estimate the subject-specific time shifts.

The restriction that γ_i, α_{0ij} and α_{1ij} each have mean zero, helps ensure identifiability, i.e. that the parameters of the model are uniquely determined. Without the random slope term α_{1ij}, our model is a simplification of the classical Shape Invariant Model (SIM) for each outcome. The SIM includes two rescaling parameters and two shift parameters. Our model excludes the SIM rescaling parameters, but includes an additional random slope term. Without the random slope term, identifiability of our model is established in [6] under the normalizing condition that shift parameters γ_i and α_{0ij} have mean zero, which we maintain. To ensure identifiability in our model with a random slope, α_{1ij}, we simply require the further restriction that the mean of α_{1ij} is zero. Following [6], the restrictions on the mean of γ_i, α_{0ij} and α_{1ij} and the assumption that g_j is a continuously differentiable monotone function for each outcome ensure identifiability.

3. The algorithm

The algorithm reduces the high dimensional and complex problem into simpler problems. Each of the unknown parameters (g_j, γ_i, α) is estimated in turn using the current estimates of the other parameters. This process is iterated until convergence of the residual sum of squares (RSS). The algorithm utilizes three different types of *partial residuals*, using the language of generalized additive model estimation [18], which we denote  ,  ,  (Table 1). If we assume the model (1) is correct then each of the partial residuals provides an unbiased estimate of one of the unknown parameters. Specifically, conditional expectations of the partial residuals are equivalent, or at least approximately equivalent, to the target parameters (Table 1). We begin the algorithm by initializing $\gamma_i = 0$ and iterating the following.

1. Given γ_i, estimate the monotone functions g_j by setting $\alpha_{0ij} = \alpha_{1ij} = 0$ and iterating the following subroutine.
   a. Estimate g_j by a monotone smooth of  .
   b. Estimate α_{0ij}, α_{1ij} by linear mixed-model of  . Repeat Steps a and b until convergence of the RSS for the jth outcome,  .
2. Given current set of g_j, set $\alpha_{0ij} = \alpha_{1ij} = \varepsilon_{ij}(t) = 0$, and estimate each γ_i with the average of  over all j and t. Repeat Steps 1 and 2 until convergence of the total residual sum of squares  .

Step 1 involves m parallel subroutines for fitting g_i and the subject-specific α_{0ij} and α_{1ij} for each outcome $j = 1,\ldots, m$. We begin each of the m parallel subroutines by setting $\alpha_{0ij} = 0$ and $\alpha_{1ij} = 0$. To estimate g_j, we use a monotone B-spline smoother [19] through the scatter plot of ($t + \gamma_i$, ). This is accomplished using the R package fda [20]. Under the model,  is independently and identically distributed about $g_j(t)$, so we need not model within-subject correlations at this step. To estimate α_{0ij} and α_{1ij}, we minimize  by fitting a linear mixed-effect model of 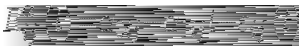 using *lme4* [21]. Steps a and b are repeated with the same γ_i until convergence of RSS_j. The result is m smooth curves, $g_1,\ldots, g_m$, and $m \times n$ sets of random effects estimates for the m outcomes and n individuals. Plots of the fits and residuals at each iteration are produced with *ggplot2* [22].

In Step 2 we invert the outcome variables and estimate the time shift parameters γ_i by taking the average of  over all outcomes and times for each individual. This is the only step that pools data derived from all outcomes at once. To down-weight the influence of more variable outcomes, one could use a weighted average with weights inversely proportional to each outcome's residual variance.

4. Simulations

Data simulated as described in Section 2 are depicted in Figure 2. We submitted these data to the algorithm. Each curve was estimated with the same monotone B-spline smoother with 5 equally spaced knots and 5th degree polynomial splines. The resulting fitted curves are shown to have good fidelity with the true logistic, linear, and quadratic curves (Panel C).

We also plotted the true simulated time shifts against the estimated time shifts (not shown). The agreement was not perfect, but as hoped, the regression line through this scatter plot lies close to the identity line. The residual sum of squares for each of the outcomes converged in 10 iterations to a tolerance of 0.1% of the residual sum of squares. Code to reproduce the results and an animation demonstrating convergence can be found at http://mdonohue.bitbucket.org/grace/.

5. ADNI and PAQUID results

Figure 3 shows longitudinal plots of some of the key variables that have been collected over the course of ADNI. Amyloid plaque accumulation in brain is associated with decreased CSF and increased Pittsburgh compound B (PiB) and florbetapir uptake on PET. Figure 3 also includes CSF tau and p-tau; FreeSurfer volumetric MRI data for hippocampal, whole brain, and ventricular volume; fluorodeoxyglucose (FDG) uptake on PET; 13 item Alzheimers Disease Assessment Scale-Cognitive Sub-scale (ADAS13) including delayed word recall and number cancellation tasks; Mini Mental State Exam (MMSE); ADCS Functional Activities Questionnaire (FAQ); Rey Auditory Visual Learning Test (RAVLT), and the Clinical Dementia Rating Scale Sum-of-Boxes (CDRSB). CSF measures were collected only on a subset of ADNI volunteers, as evidenced by the relative sparsity of CSF data. Florbetapir PET imaging and the EMCI cohort were added relatively late in the study. Additional details on these measures in ADNI are available from adni-info.org.

One of the primary motivations for this work was to derive a data driven version of the progression curves hypothesized by Jack et al. [4]. The hypothesized figure shows the key markers of disease progressing on a common vertical scale from normal to abnormal, with clinical disease stage on the horizontal scale. The percentile scale is a natural choice to attain a common scale. Therefore, before submitting ADNI measures to our algorithm, we first transformed them to a percentile scale. Since the diagnostic groups are not equally represented, we use a weighted percentile transformation. The resulting scale is percentile normalized to range from 0 (least severe observed value) to 100 (most severe observed value). Percentiles were calculated using the empirical cumulative distribution function (ECDF) derived by weighting according to the inverse of the proportion of observations from each diagnostic category (CN, EMCI, LMCI, AD). For example, in total we observed n = 7,216 MMSE scores from CN (n = 2,094/7,216 = 29.0%), EMCI (n = 979/7,216 = 14.6%), LMCI (n = 3,074/7,216 = 42.6%), and AD (n = 1,069/7,216 = 14.8%). Because diagnostic groups are not equally represented, we used the inverse proportions as weights in computing the ECDF. Table 3 provides the raw values that correspond to the resulting percentiles.

ADNI includes many CN, MCI, and even misdiagnosed probable AD who may not have AD pathology. This is because physicians do not have access to biomarker results at the time of diagnosis. These subjects do not provide any information about the long-term trends of AD. Therefore, we applied our algorithm to the subset of N = 388 ADNI participants with some evidence of abnormal accumulation of amyloid in brain ("Amyloid+") using published thresholds for CSF Aβ (192 pg/ml), PiB PET (1.5 standardized uptake value ratio [SUVR] in region relative to the cerebellum), and florbetapir PET (1.1 SUVR in region relative to the cerebellum) [23, 24, 25]. The group consisted of n = 100 CN, 137 ECMI, 225 LMCI, and 117 AD; but the algorithm was blind to these diagnostic categorizations. Following the same approach as the simulation, the B-spline smooths were fitted with 5 equally spaced knots and 5th degree polynomial splines.

The top of Figure 4a shows the estimated long-term trajectories among Amyloid+ADNI subjects. Time has been shifted so that time zero represents the time at which the mean CDRSB score reaches the 80th percentile. The resulting time scale can be interpreted as time until progression to the worst 20th percentile of CDRSB. To reduce clutter and because it was very similar to the ADAS13 trajectory, CDRSB is not shown in the middle panel. We also omit ventricular volume, which tracks closely with hippocampus. The bottom left of Figure 4a depicts the first derivatives of each curve divided by the standard deviation of its residuals. The shaded regions in the top panels of Figure 4 depict bootstrap estimates of the confidence bands. We re-sampled the subjects with replacement and re-applied the algorithm 100 times. Each re-sampled population contained the same number of subjects as the observed population. For each time point, we then took the 2.5 and 97.5 percentiles of the 100 curves as the lower and upper limits.

We also applied the algorithm to the subset of N = 570 ADNI participants who had at least one Apolipoprotein E e4 allele (Figure 4). This subgroup consisted of n = 92 CN, 85 ECMI, 248 LMCI, and 145 AD; but again the algorithm was blind to the diagnoses. Note that this group contains many subjects who would be classified as Amyloid-. Utilizing MMSE trajectories from the PAQUID study, we applied a post-processing step to transform time. The PAQUID time scale is time to onset of dementia. The ADNI time scale, with estimated subject-specific time shifts, lacks a pathological anchor. To transform the ADNI time scale to the PAQUID time to onset, we compose the ADNI MMSE trajectory with the inverse PAQUID trajectory. That is, if f denotes the estimated MMSE curve from ADNI and g denotes the same from PAQUID, with inverse g^{-1}, we transform ADNI time, t, via the composition $g^{-1}(f(t))$. Because PAQUID lacks measures of amyloid burden, we could not do this transformation with our Amyloid+ analysis.

For comparison, Figure 5 depicts trajectories estimated from those without evidence Amyloid burden and those without an ApoE ε4 allele. We used the same transformations of time as described above, in particular using estimated trajectories from PAQUID to calibrate the ADNI time scale. The Amyloid-group consisted of n = 190 CN, 153 ECMI, 92 LMCI, and 13 AD; the ApoE ε4 allele non-carrier group consisted of n = 263 CN, 124 ECMI, 219 LMCI, and 75 AD.

6. Discussion

Bateman et al. [26] recently produced estimated progression curves over a 50 year span using data from the Dominantly Inherited Alzheimer's Network (DIAN). A key feature of autosomal dominant AD is that the age of onset of symptoms is expected to be close to the age of onset of the parent. Bateman et al. [26] use the parents' ages of onset to estimate long-term disease progression from cross-sectional data from mutation carriers spanning 25 years before, to 10 years after, the parents' age of onset. In contrast, we have less confidence about the age of onset in the ADNI population of sporadic AD. Our self modeling regression approach addresses this limitation of ADNI by simultaneously estimating age of onset and the progression curves.

Simulations suggest that our iterative algorithm can recover reasonable estimates of the long-term trajectories from short-term observations. Nonparametric estimation of the monotone curves allows different shaped curves to emerge without pre-specifying parametric families. Further simulation studies and analytic development of asymptotic convergence is warranted. Convergence of estimates of the time shifts will rely in part on the abundance of outcomes. With only three outcomes used in the simulation, the algorithm estimated the time shifts surprisingly well.

Jack et al. [4, 5] proposed that all disease markers range from zero (absolutely normal) to one (absolutely abnormal) and follow sigmoid shapes. Rather than assuming this to be true and following a parametric approach, we opted to follow a nonparametric monotone smoothing approach. We chose to apply our algorithm to relatively pathologically homogenous Amyloid+ and ApoE ε4+ subsets. While restricting to Amyloid+ is ostensibly assuming that amyloid is the precursor to the AD cascade, we feel that including many subjects with a low likelihood of AD pathology may lead to distorted trajectories. The ApoE ε4 allele is the major genetic risk factor for sporadic AD, though roughly one third of individuals with AD do not carry it.

Our nonparametric approach does not assume sigmoid curves, but rather a very flexible class of monotone curves. Surprisingly, among Amyloid+ subjects, we found mean CSF Aβ follows a linear trajectory, while tau, p-tau, and PiB PET follow sigmoid shapes. However, the sigmoid shapes are flatter than those proposed by [4], and remain within the 40 to 80th percentile range. Glucose metabolism (FDG PET), hippocampal volume, ventricular volume, learning, and cognition (ADAS13) all track very close to each other in near linear trajectories. Function (FAQ) was the final domain to fail following a parabolic trajectory. It is quite possible that ADNI does not have enough data from later stage dementia, which might demonstrate the final plateau of a sigmoid. The relative paucity of available observations at the most severe stage of disease is limitation than will be addressed as the model is expanded to include additional datasets.

The question of which markers become abnormal first is distinct from the question of which markers can be efficiently estimated in terms of the signal-to-noise ratio. To explore the latter question, we provide plots of the first derivatives of curves divided by the residual standard deviation. Hippocampal volume appears to dominate the other measures across the

15 year span in both analyses, with the possible exception of CSF markers. The CSF markers show some areas of relative high standardized slopes, but these could be due to scant data and spurious acceleration near the boundaries of observation (bottom Figure 5). In other cases, the CSF measures are relatively flat which may cause spurious acceleration depicted in the bell shapes (bottom Figure 4a).

Our approach also does not assume that the mean should attain zero and one. Without this assumption, our algorithm demonstrates much pathological heterogeneity or measurement variability, even in the selected Amyloid+ subset. For instance, 15 years prior to reaching the worst 20th percentile of CDRSB, CSF Aβ ranges between zero and the 80th percentile, with a mean at about the 20th percentile. Between-subject variability tends to flatten the mean trajectory, such that most estimated trajectories in Figure 4a do not cover the full range from zero to one. Assuming the mean attains zero and one may oversimplify the heterogeneous reality of the disease cascade at the population level.

Perhaps some of the heterogeneity can be explained by diet, lifestyle, education, occupation, or other covariates related to cognitive reserve. Genetics or family history might also explain heterogeneity. We plan to investigate these hypotheses in the future by building covariates into the model, but more data on the earliest phases of the disease will be necessary. Fortunately, the mixed-model framework we have adopted is well suited to pooling datasets for meta-analyses. Hierarchical random effects can be used to model within-study as well as within-subject correlation. Meta-analyses may also help address a key limitation of the ADNI data, which is the age range of ADNI participants is restricted to 55 to 95 years at baseline. In fact, across our 15 year span of estimated long-term progression, the mean age of subjects represented remains in the 70 to 75 year range. Clearly we need to incorporate data from younger cohorts.

The comparison groups depicted in Figure 5 are difficult to interpret. Note that only n =13 out of 130 (10%) of AD subjects with known amyloid status are classified as Amyloid- and n = 75 out of 220 (34%) of AD subjects have no ApoE ε4 allele. Also many of the subjects with mild or no impairment entered into this analysis may never progress. However, we might interpret the Amyloid-trajectories as a representation of non-Alzheimer's pathology which is marked by divergent biomarker signature, including normal CSF and less pronounced hippocampal atrophy and ventricular expansion. In contrast, the ApoE ε4 non-carrier group appears to converge toward the ApoE ε4 carrier group as symptom progress. This apparent convergence is possibly due to the concatenation of subjects without Alzheimer's pathology antecedent to those with Alzheimer's pathology rather than a true acceleration of pathology in ApoE ε4 non-carriers.

Our analysis suggests that amyloid PET imaging with florbetapir or PiB may reach abnormal levels first, followed by CSF tau and p-tau. This is consistent with the view that PET imaging is the most direct measure of amyloid accumulation in brain (generally considered to be the inciting event in AD), and suggests a delay before abnormalities are observed in "downstream" markers of neurodegeneration in the CSF. Learning, glucose metabolism, hippocampal atrophy, and cognition all follow in close succession. Function is the last domain to progress to abnormality, as expected. Plots of the adjusted slopes indicate

that hippocampal volume assessed by structural MRI provides the most efficient measure of disease progression across the full span. These observations are consistent with our current understanding of the disease and paint a picture in general agreement with the [4] model. Our approach will facilitate analyses utilizing diverse datasets with overlapping measures, providing a framework for validating models of disease progression.

Finally, our framework provides an approach to assessing the growing body of outcome data, providing quantitative data to inform still-hypothetical biomarker models. As noted in an editorial accompanying the revised model from [5, 27], biomarker modeling will be facilitated by ongoing accrual of data that reduces the gaps in our observations; this applies to both hypothetical and data-driven efforts.

Acknowledgments

We would like to acknowledge the invaluable contributions of our PAQUID and ADNI collaborators, co-investigators, volunteers, and their families.

Funding: This work was support by a grant (1KL2RR031978) from the National Institutes of Health funded University of California, San Diego Clinical and Translation Research Institute (1UL1RR031980). Data collection and sharing for this project was funded by the Alzheimer's Disease Neuroimaging Initiative (ADNI) (U01 AG024904). ADNI is funded by the National Institute on Aging, the National Institute of Biomedical Imaging and Bioengineering, and through generous contributions from the following: Abbott; Alzheimers Association; Alzheimers Drug Discovery Foundation; Amorfix Life Sciences Ltd.; AstraZeneca; Bayer HealthCare; BioClin-ica, Inc.; Biogen Idec Inc.; Bristol-Myers Squibb Company; Eisai Inc.; Elan Pharmaceuticals Inc.; Eli Lilly and Company; F. Hoffmann-La Roche Ltd and its affiliated company Genentech, Inc.; GE Healthcare; Innogenetics, N.V.; IXICO Ltd.; Janssen Alzheimer Immunotherapy Research & Development, LLC.; Johnson & Johnson Pharmaceutical Research & Development LLC.; Medpace, Inc.; Merck & Co., Inc.; Meso Scale Diagnostics, LLC.; Novartis Pharmaceuticals Corporation; Pfizer Inc.; Servier; Synarc Inc.; and Takeda Pharmaceutical Company. The Canadian Institutes of Health Research is providing funds to support ADNI clinical sites in Canada. Private sector contributions are facilitated by the Foundation for the National Institutes of Health (www.fnih.org). The grantee organization is the Northern California Institute for Research and Education, and the study is coordinated by the Alzheimer's Disease Cooperative Study at the University of California, San Diego. The Laboratory for Neuroimaging at the University of Southern California disseminates ADNI data. This research was also supported by NIH grants P30 AG010129 and K01 AG030514. Novartis and IPSEN laboratories, and Conseil Regional dAquitaine fund PAQUID.

References

[1]. Lindstrom MJ, Bates DM. Nonlinear mixed effects models for repeated measures data. Biometrics. 1990; 46:673–687. [PubMed: 2242409]

[2]. Pinheiro, J.; Bates, D.; DebRoy, S.; Sarkar, D.; R Core Team. nlme: Linear and Nonlinear Mixed Effects Models. 2012. R package version 3.1-106

[3]. Pinheiro, JC.; Bates, DM. Mixed-effects models in S and S-PLUS. Springer Verlag; 2000.

[4]. Jack CR, Knopman DS, Jagust WJ, Shaw LM, Aisen PS, Weiner MW, Petersen RC, Trojanowski JQ. Hypothetical model of dynamic biomarkers of the Alzheimer's pathological cascade. The Lancet Neurology. 2010; 9:119–128. [PubMed: 20083042]

[5]. Jack CR, Knopman DS, Jagust WJ, Petersen RC, Weiner MW, Aisen PS, Shaw LM, Vemuri P, Wiste HJ, Weigand SD, Lesnick TG, Pankratz VS, Donohue MC, Trojanowski JQ. Tracking pathophysiological processes in Alzheimer's disease: an updated hypothetical model of dynamic biomarkers. The Lancet Neurology. 2013; 12:207–216. [PubMed: 23332364]

[6]. Kneip A, Gasser T. Convergence and consistency results for self-modeling nonlinear regression. The Annals of Statistics. 1988; 16:82–112.

[7]. Lawton WH, Sylvestre EA, Maggio MS. Self modeling nonlinear regression. Technometrics. 1972; 14:513–532.

[8]. Ladd WM, Lindstrom MJ. Self-modeling for two-dimensional response curves. Biometrics. 2000; 56:89–97. [PubMed: 10783781]

[9]. Brumback LC, Lindstrom MJ. Self modeling with flexible, random time transformations. Biometrics. 2004; 60:461–470. [PubMed: 15180672]

[10]. Beath KJ. Infant growth modelling using a shape invariant model with random effects. Statistics in Medicine. 2007; 26:2547–2564. [PubMed: 17061310]

[11]. Lindstrom MJ. Self-modeling with random shift and scale parameters and a free-knot spline shape function. Statistics in Medicine. 1995; 14:2009–2021. [PubMed: 8677401]

[12]. Wang Y, Ke C, Brown MB. Shape-invariant modeling of circadian rhythms with random effects and smoothing spline anova decompositions. Biometrics. 2003; 59:804–812. [PubMed: 14969458]

[13]. Altman N, Villarreal J. Self-modelling regression for longitudinal data with time-invariant covariates. Canadian Journal of Statistics. 2004; 32:251–268.

[14]. Coull BA, Staudenmayer J. Self-modeling regression for multivariate curve data. Statistica Sinica. 2004; 14:695–711.

[15]. Telesca D, Inoue LYT. Bayesian hierarchical curve registration. Journal of the American Statistical Association. 2008; 103:328–339.

[16]. Dartigues JF, Gagnon M, Barberger-Gateau P, Letenneur L, Commenges D, Sauvel C, Michel P, Salamon R. The PAQUID epidemiological program on brain aging. Neuroepidemiology. 1992; 11:8.

[17]. Amieva H, Le Goff M, Millet X, Orgogozo JM, Peres K, Barberger-Gateau P, Jacqmin-Gadda H, Dartigues JF. Prodromal Alzheimer's disease: Successive emergence of the clinical symptoms. Annals of Neurology. 2008; 64:492–498. [PubMed: 19067364]

[18]. Hastie T, Tibshirani R. Generalized additive models. Statistical Science. 1986; 1:297–310.

[19]. Ramsay JO. Estimating smooth monotone functions. Journal of the Royal Statistical Society. Series B, Statistical Methodology. 1998; 60:365–375.

[20]. Ramsay, JO.; Wickham, H.; Graves, S.; Hooker, G. fda: Functional Data Analysis. 2012. R package version 2.2.8

[21]. Bates, D.; Maechler, M.; Bolker, B. lme4: Linear mixed-effects models using S4 classes. 2012. R package version 0.999999-0

[22]. Wickham, H. ggplot2: elegant graphics for data analysis. Springer New York: 2009.

[23]. Shaw LM, Knapik-Czajka M, Lee VMY, Trojanowski JQ, Vander-stichele H, Clark CM, Aisen P, Petersen R, Blennow K, Soares H, Simon A, Potter W, Lewczuk P, Dean R, Siemers E. Cerebrospinal fluid biomarker signature in Alzheimer's Disease Neuroimaging Initiative subjects. Annals of Neurology. 2009; 65:403–413. [PubMed: 19296504]

[24]. Jack CR, Lowe VJ, Senjem ML, Weigand SD, Kemp BJ, Shiung MM, Knopman DS, Boeve BF, Klunk WE, Mathis CA, Petersen RC. 11C PiB and structural MRI provide complementary information in imaging of Alzheimer's disease and amnestic mild cognitive impairment. Brain. 2008; 131:665–680. [PubMed: 18263627]

[25]. Jagust W, Landau S, Shaw L, Trojanowski J, Koeppe R, Reiman E, Foster N, Petersen R, Weiner M, Price J, Mathis C. Relationships between biomarkers in aging and dementia. Neurology. 2009; 73:1193–1199. [PubMed: 19822868]

[26]. Bateman RJ, Xiong C, Benzinger TL, Fagan AM, Goate A, Fox NC, Marcus DS, Cairns NJ, Xie X, Blazey TM, Holtzman DM, San-tacruz A, Buckles V, Oliver A, Moulder K, Aisen PS, Ghetti B, Klunk WE, McDade E, Martins RN, Masters CL, Mayeux R, Ringman JM, Rossor MN, Schofield PR, Sperling RA, Salloway S, Morris JC. Clinical and biomarker changes in dominantly inherited Alzheimer's disease. New England Journal of Medicine. 2012; 367:795–804. [PubMed: 22784036]

[27]. Frisoni GB, Blennow K. Biomarkers for Alzheimer's: the sequel of an original model. The Lancet Neurology. 2013; 12:126–128. [PubMed: 23332358]

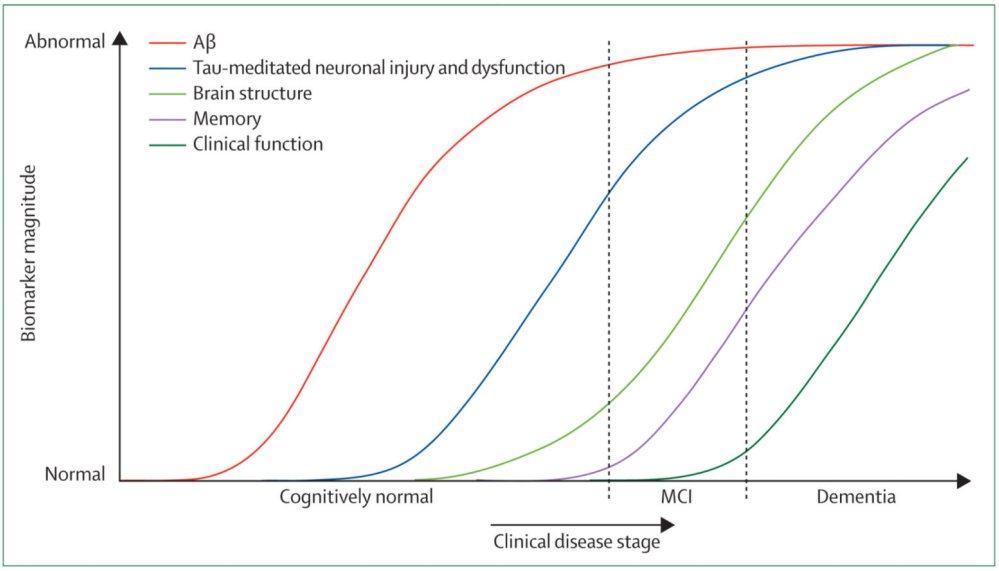

Figure 1.
Dynamic biomarkers of the AD cascade hypothesized by Jack et al.[4].

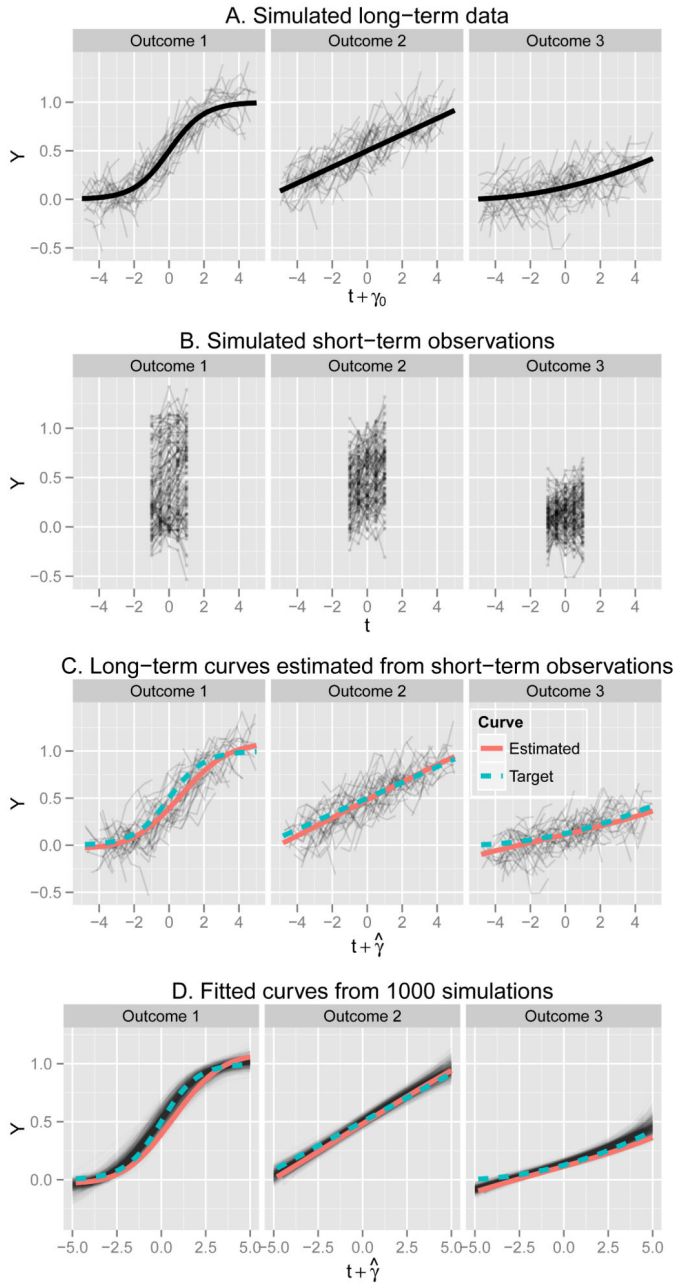

Figure 2.

Panel A. The three monotone functions depicted in bold are logistic, linear, and quadratic. Long-term trends are easily apparent because data is plotted with the unknown time shifts. The simulated data is not derived from real data and is intended for demonstration only. **Panel B.** Long-term trends are obscured because we observe the data in the short-term, without the unknown time shifts. **Panel C.** The algorithm described in Section 3 estimates long-term curves (red line) with good fidelity to the true target curves (dashed green line). **Panel D.** We repeated the experiment, generating new data and fitting the curves, 1000 times and plot the fitted curves in black.

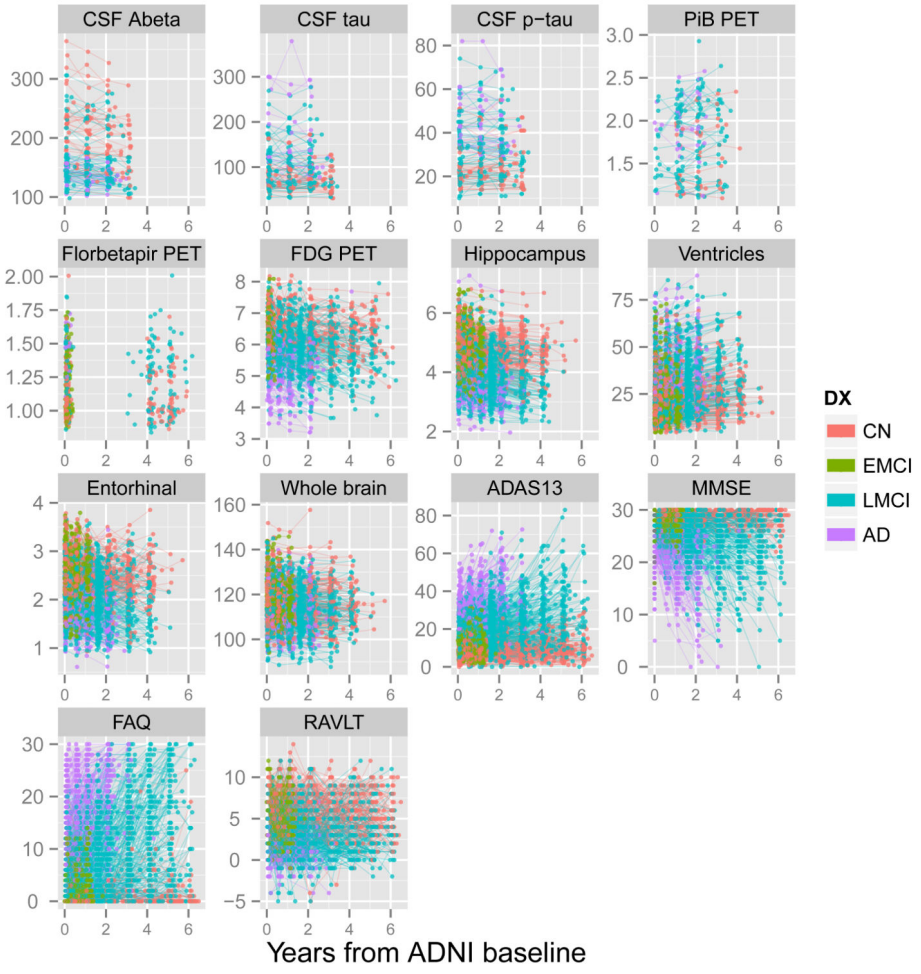

Figure 3.

The ADNI battery consists of a rich panel of biomarkers and assessments collected at six month intervals for up to 6 years. Subjects were entered into one of four diagnostic categories. The EMCI cohort was enrolled relatively recently. CSF measures are not collected from every ADNI volunteer. Some measures, such as florbetapir PET, have not been collected for as long. There is no obvious biological or clinical reference time point. The *x*-axis is time since first ADNI visit.

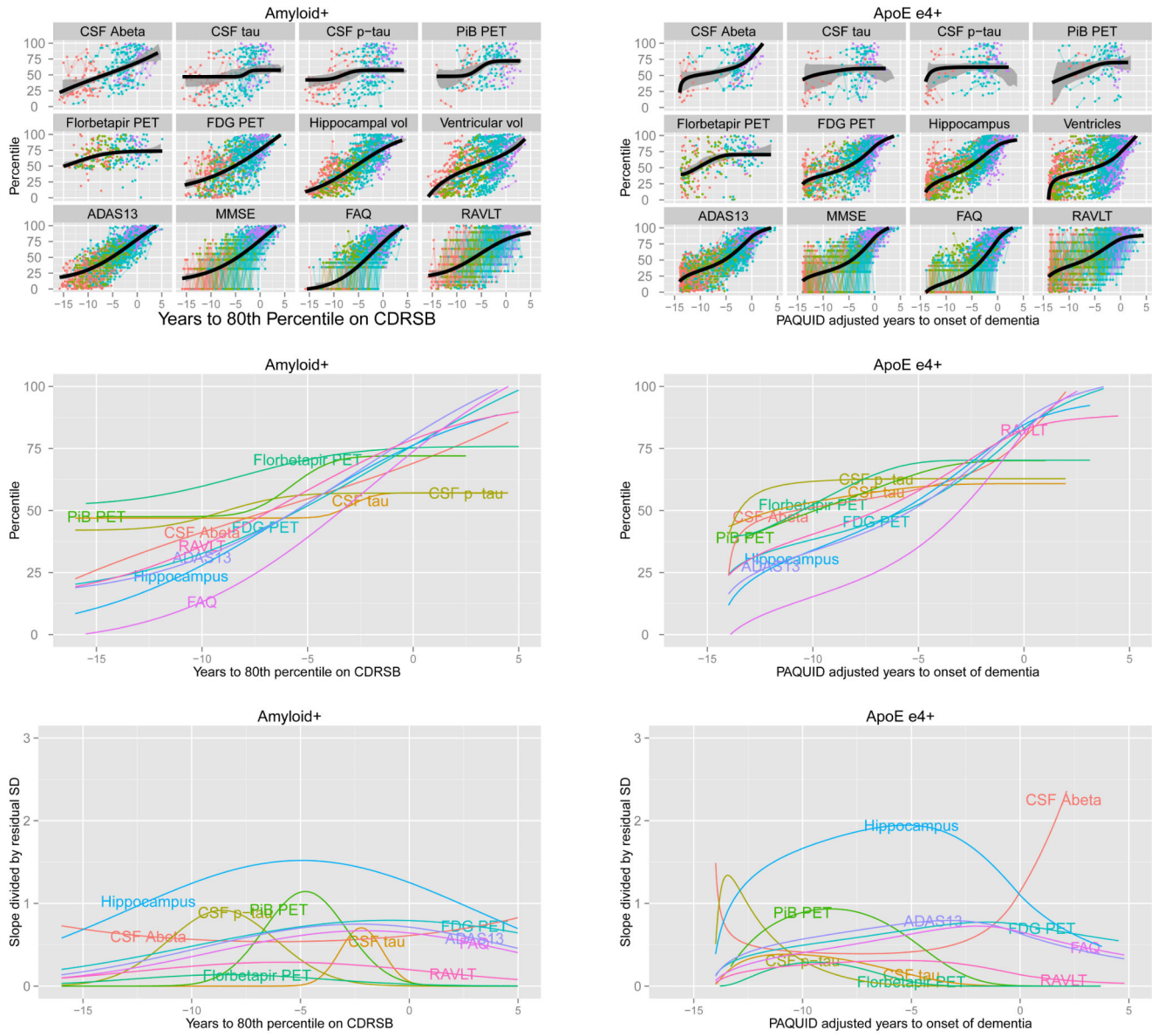

(a) **ADNI Amyloid+ subjects.** (b) **ADNI ApoE ε4 allele carriers.**

Figure 4.

The top panels show each of the mean trajectories superimposed over the subject-level observations from N = 579 Amyloid+ and N = 570 ApoE e4 individuals colored by diagnosis. Colors in the top panel represent diagnosis at ADNI baseline, CN, EMCI, LMCI, and AD, and are generally sorted as expected. Shaded gray regions, where visible in the top panels, represent bootstrap 95% confidence bands. The middle panels show all of the trajectories at once. On the left, time has been shifted so that time zero represents the time at which mean CDRSB trajectory (not shown) meets the 80th percentile. On the right, time has been adjusted using long-term PAQUID MMSE trajectories so that time zero represents the

estimated time to onset of dementia. The bottom panels show rates of change standardized by residual standard deviation.

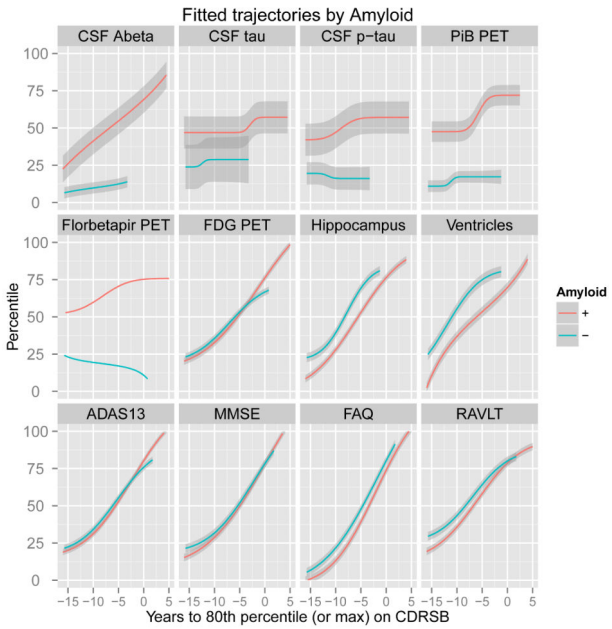

(a) **Amyloid+ vs. Amyloid-.**

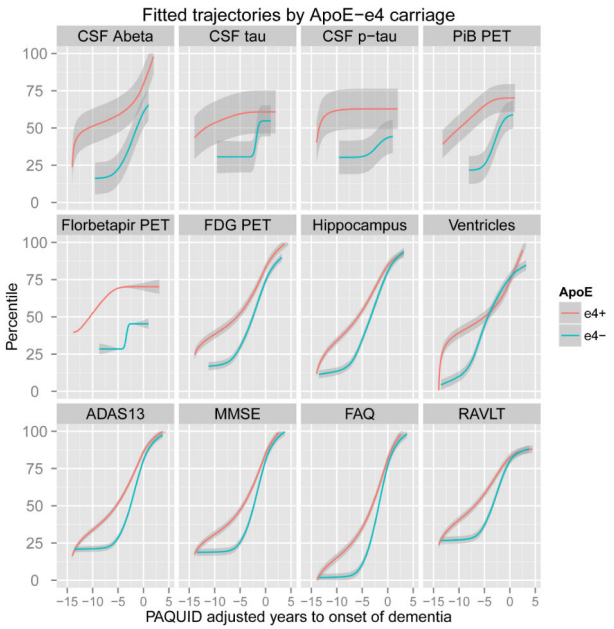

(b) **ApoE ε4 allele carriers vs non-carriers.**

Figure 5.

Each panel repeats the same estimated trajectories in the Amyloid+ and ApoE ε4 carrier groups, as in Figure 4, and includes the Amyloid- and ApoE ε4 non-carrier comparison groups. The Amyloid-group consisted of n = 190 CN, 153 ECMI, 92 LMCI, and 13 AD; the ApoE ε4 allele non-carrier group consisted of n = 263 CN, 124 ECMI, 219 LMCI, and 75 AD. Shaded gray regions represent 95% confidence bands derived analytically, rather than by the bootstrap as in Figure 4.

Table 1

Partial residuals for each target parameters and their conditional expectations. Target parameters of our model and the partial residuals we use to estimate each parameter in the iterative algorithm. Under the assumptions of the model, we see that the conditional expectations of the partial residuals are equivalent to the parameters of interest. The equivalence is approximate for 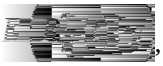 , since here we integrate over the function  . The approximation is reasonable provided a_{0ij}, a_{1ij}, ε_{ij} are small and  is not too steep.

Partial Residual	Conditional Expectation
Long-term smooth curve: g_j	
$R^{g}_{ij}(t) = Y_{ij}(t) - a0ij - a1ijt$	$E(R^{g}_{ij}(t) \mid g_j, t, \gamma_i) = g_j(t+\gamma_i)$
Subject- & outcome-specific intercept & slope: a_{0ij}, a_{1ij}	
$R^{a}_{ij}(t) = Y_{ij}(t) - g_j(t+\gamma_i)$	$E(R^{a}_{ij}(t) \mid a0ij, a1ij, t) = a0ij + a1ijt$
Subject-specific time shift: γ_i	
$R^{\gamma}_{ij}(t) = t - g_j^{-1}(Y_{ij}(t))$	$E(R^{\gamma}_{ij}(t) \mid \gamma_i) \approx g_j^{-1}(g_j(t+\gamma_i)) - t = \gamma_i$

Table 2

The number of subjects and observations available in the ADNI dataset varies by outcome. The table above provides counts of the number of subjects and observations available for each of the outcomes.

n/N *	CN	EMCI	LMCI	AD	Total
CSF tau (pg/ml)	36/132		54/211	16/63	106/406
CSF p-tau (pg/ml)	36/132		54/211	16/63	106/406
CSF A-beta (pg/ml)	36/132		54/211	16/63	106/406
PiB PET (SUVR)	19/49		65/141	19/34	103/224
Florbetapir PET (SUVR)	270/270	290/290	252/252	98/98	910/910
FDG PET (uptake)	345/763	299/346	409/1263	208/434	1261/2806
Ventricles (%ICV)	413/1448	298/852	548/1927	267/637	1526/4864
Hippocampus (%ICV)	413/1448	298/852	548/1927	267/637	1526/4864
ADAS13	418/1883	305/825	560/2735	309/871	1592/6314
MMSE	608/2094	450/979	864/3074	474/1069	2396/7216
FAQ	416/1891	304/823	560/2781	310/907	1590/6402
RAVLT	419/1893	306/825	560/2739	312/884	1597/6341

* Total number of subjects *n* and observations *N*.

Table 3

Each of the ADNI outcomes was transformed to a common percentile scale. Percentiles were calculated using the empirical cumulative distribution function (ECDF) weighted according to the inverse of the proportion of observations from each diagnostic category (CN, EMCI, LMCI, AD). Increasing percentile scores are intended to be associated with worsening of the disease. Here we provide the raw values associated with the given percentile values.

	Percentiles of key ADNI outcomes					
	n/N *	**0th**	**25th**	**50th**	**75th**	**100th**
CSF tau (pg/ml)	106/406	31	64	90	122	379
CSF p-tau (pg/ml)	106/406	10.0	21.6	32.3	42.0	82.0
CSF A-beta (pg/ml)	106/406	364	181	146	131	98
PIB PET (SUVR)	103/224	1.09	1.36	1.85	2.09	2.93
Florbetapir PET (SUVR)	910/910	0.83	1.01	1.21	1.41	2.01
FDG PET (uptake)	1261/2806	8.54	6.56	6.06	5.50	3.20
Ventricles (%ICV)	1526/4864	0.45	1.67	2.44	3.40	9.03
Hippocampus (%ICV)	1526/4864	0.79	0.50	0.43	0.36	0.20
ADAS13	1592/6314	0.00	9.23	15.91	26.26	85.00
MMSE	2396/7216	30.0	29.2	27.5	24.4	0.0
FAQ	1590/6402	0.00	0.73	4.04	12.87	30.00
RAVLT (Trial 5 minus Trial 1)	1597/6341	14.00	6.37	4.08	2.18	−5.00

* Total number of subjects *n* and observations *N*.